

Synthesis, Crystal Structure, and Physical Properties of BaSnS₂

Wilarachchige D. C. B. Gunatilleke, Andrew F. May, Angela R. Hight Walker, Adam J. Biacchi, and George S. Nolas*

Phase-pure $BaSnS_2$, with space group $P2_1/c$, is synthesized, and the structural and physical properties are investigated. Thermal properties and optical measurements are reported for the first time. The Debye temperature and Sommerfeld coefficient are obtained from temperature-dependent heat capacity measurements, the latter indicating that $BaSnS_2$ is an electrical insulator. A direct bandgap of 2.4 eV is obtained from diffuse reflectance and photoluminescence spectroscopy. The findings herein lay the foundation for understanding the physical properties of this material and are part of a continuing effort to investigate previously unexplored ternary chalcogenides.

1. Introduction

Metal chalcogenides continue to be investigated for diverse applications of interest, including nonlinear optics, [1] thermoelectrics, [2,3] superconductivity, [4] and ferroelectrics. [5] More recently, the synthesis and physical properties of ternary^[6,7] and quaternary^[8-11] chalcogenides have been of intense interest, not only due to an interest in their fundamental properties but also for applied research toward energy-related applications. [12–16] For certain materials, the electrical properties can be modified by a variation in stoichiometry, [17-19] while others display transport properties that are atypical of compositions in this class of materials. [20,21] Wide bandgap semiconductor chalcogenides continue to be of interest due to their interest in a broad range of technological applications. [22] Certain compositions have also been synthesized in the nanocrystalline form to investigate the effects of nano-structuring on the transport properties.[23,24]

W. D. C. B. Gunatilleke, G. S. Nolas Department of Physics University of South Florida Tampa, FL 33620, USA E-mail: gnolas@usf.edu

A. F. May Materials Science and Technology Division Oak Ridge National Laboratory Oak Ridge, TN 37831, USA

A. R. H. Walker, A. J. Biacchi Nanoscale Device Characterization Division National Institute of Standards and Technology (NIST) Gaithersburg, MD 20899, USA

The ORCID identification number(s) for the author(s) of this article can be found under https://doi.org/10.1002/pssr.202100624.

DOI: 10.1002/pssr.202100624

Many of the achievements outlined earlier have advanced our understanding of the material formation and synthetic methodologies. In addition, investigations into specific structure–property relationships can now be realized by predictive computamethods.[25] and modeling tional Furthermore, chalcogenide compositions possess physical properties that are desirable for a variety of applications. In particular, alkali-earth-containing chalcogenide materials are of interest for highperformance photovoltaic devices. [26-33] The tunability of the electrical properties

for several different alkali-earth ternary chalcogenides has been explored both theoretically and experimentally. [34-37] Although theoretically predicted as stable phases, several compositions have yet to be confirmed experimentally. The synthetic methodology in obtaining phase-pure materials is an important step in exploring the physical properties of new materials that are of interest for technological applications. Compositions that are often seemingly simple to synthesize are, in fact, not readily obtained in phase-pure form, or have been reported to form in different structure types. One example of the latter case is BaSnS₂. It has been reported to form in different structure types, e.g., $P2_1/c^{[34]}$ and $Pnma^{[38]}$ although both these reports describe very similar synthetic approaches. Moreover, to the best of our knowledge, the physical properties of this material have not been previously reported. Herein, we report on the synthesis, thermal, and optical properties of BaSnS2. When employing the reported synthetic procedures, phase-pure BaSnS2 was not obtained; therefore, substantial effort was involved in developing the synthetic procedure described later.

2. Results and Discussion

Figure 1a shows the X-ray diffraction (XRD) refinement profiles, including the observed, calculated, and different patterns for phase-pure BaSnS₂. **Table 1** shows a summary of the Rietveld refinement results, and the atomic coordinates and isotropic thermal displacement parameters are shown in **Table 2**. The powder XRD indicated the preferred orientation of grains, presumably due to the plate-like morphology of the grains as shown in the scanning electron microscopy (SEM) analysis described later, and was therefore included in the structure refinements. The crystal structure, shown in Figure 1b, can be thought of as a modified BaS rock salt structure with each of the Ba atoms bonded to six S atoms in an ideal octahedral geometry. In this



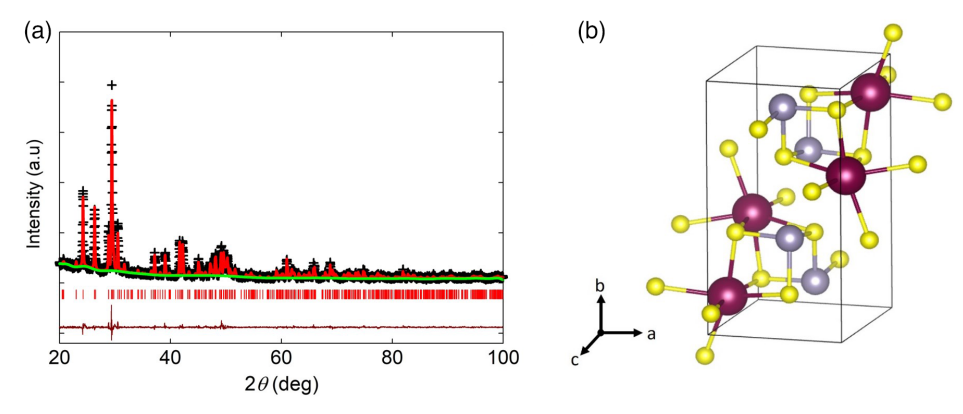


Figure 1. a) Powder XRD data for BaSnS₂, including profile fit, profile difference, and Bragg positions for the monoclinic structure that crystallizes in space group $P2_1/c$ (#14). b) Unit cell of BaSnS₂ with Ba (maroon), Sn (gray), and S (yellow).

Table 1. Crystallographic information and results from Rietveld refinement for BaSnS₂.

Phase BaSnS₂ Space group $P2_1/c$ (#14) a [Å] 6.0921(13) b [Å] 12.1617(19) c [Å] 6.2462(14) 97.041(4) β [°] $V [Å^3]$ 459.29(22) Radiation Graphite monochromated Cu Kα (1.54056 Å) $D_{\rm cal} [\rm g \, cm^{-3}]$ 4.6298 20-100 2θ range [°] Preferred orientation (010), (210), (240) planes 0.09975, 0.07717 wR_n, R_n 1.432 Goodness of fit

Table 3. Selected atomic bond distances (Å) and atomic bond angles ($^{\circ}$) for BaSnS₂.

| Bond distance | es | Bond angles | | |
|---------------|------------|-------------|------------|--|
| S1-Sn | 2.642(19) | S1-Sn-S2 | 96.1(7) | |
| S1-Ba | 3.124(19) | S1-Sn-S2 | 98.7(5) | |
| S1-Ba | 3.157(18) | S2-Sn-S2 | 92.0(4) | |
| S1-Ba | 3.224(18) | S1-Ba-S1 | 166.86(28) | |
| S1-Ba | 3.059(18) | S1-Ba-S1 | 90.7(6) | |
| S2-Sn | 2.643 (14) | S1-Ba-S1 | 90.6(6) | |
| S2-Sn | 2.677(18) | S1-Ba-S1 | 87.7(6) | |
| S2-Ba | 3.277(19) | S1-Ba-S1 | 93.7(5) | |
| S2-Ba | 3.089(20) | S1-Ba-S1 | 167.5(8) | |
| Sn-S1 | 2.642(19) | S1-Ba-S2 | 86.9(5) | |
| Sn-S2 | 2.643 (14) | S1-Ba-S2 | 81.0(5) | |
| Sn-S2 | 2.677(18) | S1-Ba-S2 | 118.3(5) | |

Table 2. Atomic coordinates, occupancy, f, and atomic displacement parameter, $U_{\rm iso}({\rm \mathring{A}}^2)$, for BaSnS₂.

| Atom | Site | X | γ | Z | f | U_{iso} |
|------------|------|------------|------------|-------------|---|-----------|
| Ва | 4e | 0.0585(11) | 0.3778(6) | 0.2573 (10) | 1 | 0.037 (5) |
| Sn | 4e | 0.5510(12) | 0.1282(5) | 0.3047(9) | 1 | 0.036 (5) |
| S 1 | 4e | 0.1149(32) | 0.1226(18) | 0.2773 (26) | 1 | 0.016 (6) |
| S2 | 4e | 0.5910(30) | 0.3409(11) | 0.3869(27) | 1 | 0.011 (6) |

way, BaSnS₂ can be obtained if every other Ba atom in the crystal lattice was replaced by Sn, resulting in a distortion of the ideal octahedral geometry surrounding Ba due to the heterogeneous bonding to each of the Ba atoms. Although Sn is occupying an octahedral site in the structure, the Sn atoms are only bonded to three other S atoms in a trigonal pyramidal local geometry. The 5s² valence electrons form a lone pair to complete a tetrahedron that contains S atoms at the other vertices. Selected bond distances and angles are shown in **Table 3**. The bond distances range

from 3.059(18) to 3.277(19) Å and from 2.642(19) to 2.677(18) Å for Ba–S and Sn–S, respectively. These bond distances are typical for Ba–S bonds of octahedrally coordinated $\rm Ba^{2+}$ atoms, such as in $\rm Ba_5Cu_8In_2S_{12},^{[39]}$ and Sn–S bonds for trigonally coordinated $\rm Sn^{2+}$ atoms, such as in $\rm Ba_7Sn_5S_{15}.^{[40]}$

Figure 2 shows an SEM image and elemental mapping from energy-dispersive spectroscopy (EDS) of part of the surface of BaSnS₂. The EDS analyses indicated that the specimen was homogeneous and confirmed the stoichiometric composition obtained from our refinement results. The SEM image shows that the grains are microcrystalline and plate-like. **Figure 3** shows differential thermal analysis (DTA) data indicating the thermal stability of BaSnS₂. Powder XRD of BaSnS₂ after DTA up to 800 K revealed Ba₃Sn₂S₇ and BaSn₃S₂ in addition to BaSnS₂, indicating the partial decomposition of the main phase above this temperature. Isobaric heat capacity, C_p , data are shown in **Figure 4**. The data approaches the Dulong–Petit limit at room temperature, an indication that the optic and acoustic mode frequencies are fully excited by this temperature. The Debye temperature, θ_D , can be calculated from the low-temperature limit of the Debye model, $C_p = \gamma T + \beta T^3$, where



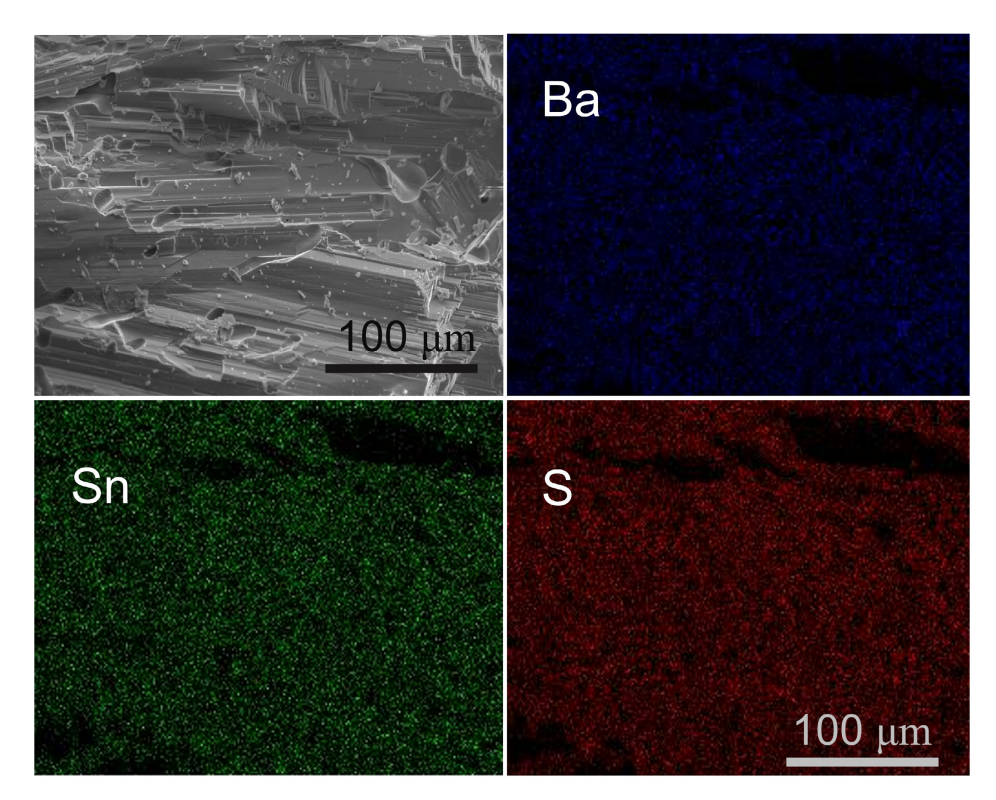


Figure 2. SEM and EDS elemental mapping of a cracked surface of a representative piece of $BaSnS_2$. All three elemental mapping images show empty dark areas in the same positions due to the difference in depth of these regions as compared to the rest of the image area.

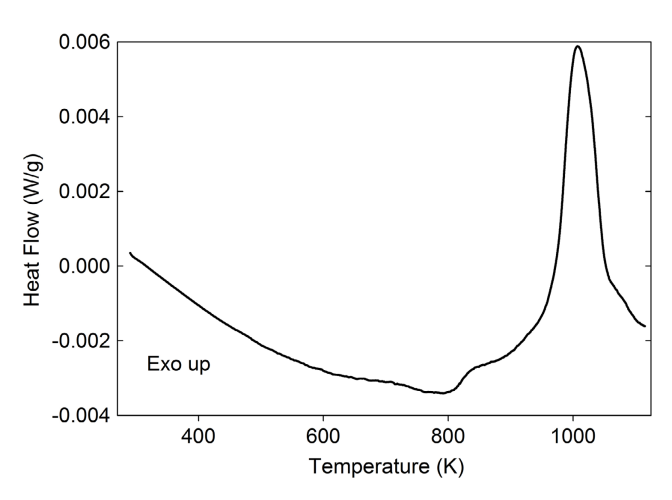


Figure 3. DTA data for BaSnS₂.

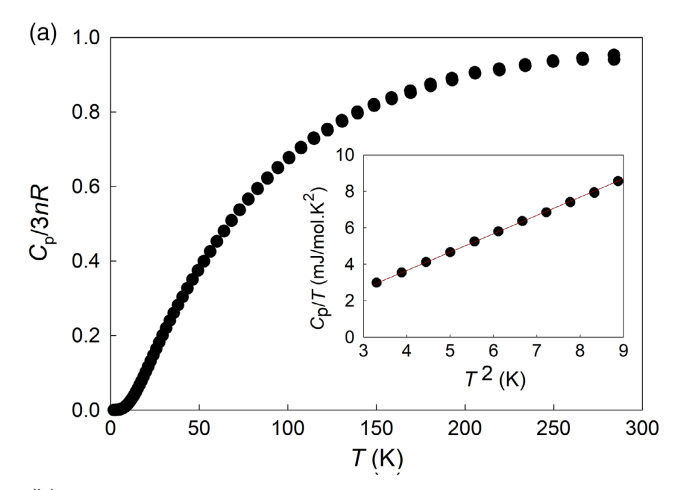
T is the absolute temperature, γ is the Sommerfeld coefficient of the electronic contribution to C_p , and β is the lattice contribution. The density of states at the Fermi level, $N(E_F)$, can be estimated from the Sommerfeld coefficient by the relation^[41]

$$\gamma = \frac{\pi^2}{3} k_B^2 N(E_F) (1 + \lambda_{e-ph})$$
 (1)

where $\gamma=0.04\,\mathrm{mJ\,mol^{-1}K^{-2}}$ from our data fit, k_B is the Boltzmann constant, and $\lambda_{\varepsilon-ph}$ is the electron–phonon coupling

constant, assumed to be zero as a first approximation, resulting in $N(E_F) = 0.04 \,\mathrm{eV}^{-1}$ per formula unit. This basically null value is typical of electrical insulators. The inset in Figure 4a shows a fit to the low-temperature data resulting in $\theta_D = 198$ K by employing $\theta_{\rm D} = (12\pi Rn/5\beta)^{1/3}$, where R is the molar gas constant and n is the number atoms per formula unit. Deviation from Debye-like behavior is observed at intermediate temperatures, as shown in Figure 4b. From this figure, C_p/T^3 versus T shows a peak at low temperature, indicating the influence of optical modes. This peak can be associated with optic modes, at approximately one-fifth of the characteristic Einstein temperature, with an effective Einstein temperature of 59 K, the occurrence of which can be attributed to the preponderance of Einstein-like modes. Lone-pair electrons, required to form the trigonal pyramid in BaSnS₂, as well as trigonal bipyramidal local environments in the case of other chalcogenide materials, can be sources of low-frequency modes. [42-46] Theoretical investigations would be useful in elucidating further insight.

To further investigate the insulating behavior indicated by the low-temperature $C_{\rm p}$ data, diffuse reflectance and photoluminescence spectroscopy were employed. Diffuse reflectance data were collected on a film of BaSnS₂ powder starting in the near-IR region and extending to the UV region. The absorption band edge was observed to begin at \approx 700 nm, as shown in **Figure 5**. A Tauc plot was constructed (inset in Figure 5) using the Kubelka–Munk transform of the diffuse reflectance plotted as a function of photon energy, $h\nu$, where h is the Planck's constant and ν is the frequency. [47] Linear fitting of



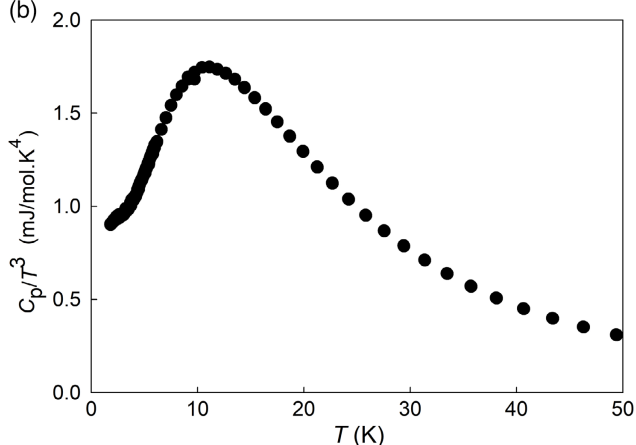


Figure 4. a) Temperature-dependent C_p for BaSnS $_2$ with the inset showing C_p/T versus T^2 data at low temperatures, where the solid line is a fit of the form $C_p/T = \gamma + \beta T^2$ and b) C_p/T^3 versus T for BaSnS $_2$ illustrating deviation from Debye-like behavior at low temperature.

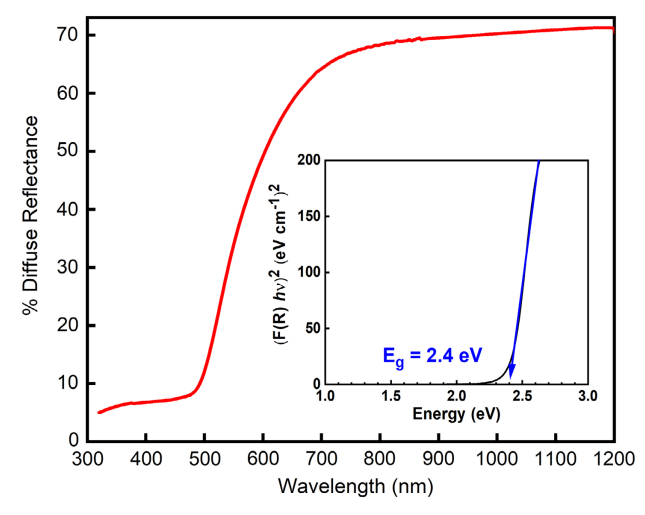


Figure 5. UV–vis–NIR diffuse reflectance spectrum of $BaSnS_2$ with corresponding Tauc plot of the Kubelka–Munk function (inset), indicating a direct bandgap of 2.4 eV.

the steepest gradient provided an estimate of 2.4 eV for the photonic bandgap. The good linear fit found with the square of the Kubelka–Munk function is indicative of a direct electron transition between the conduction and valence bands. The observation of a direct bandgap was confirmed by photoluminescence spectroscopy, which detected broad visible light emission when excited with a 514.5 nm laser, peaking at 755 nm.

3. Conclusions

In conclusion, phase-pure microcrystalline $BaSnS_2$ was synthesized. The ternary chalcogenide forms in a monoclinic crystal structure and is stable up to 925 K. Heat capacity data indicated $\theta_D = 198$ K with contributions of Einstein-like optic modes at 59 K. The insulating behavior implied by the very small electronic contribution to heat capacity was confirmed by optical measurements and revealed a direct bandgap of 2.4 eV. These results contribute toward the fundamental understanding of the physical properties of this material, and will aid in the developments of this as well as similar ternary chalcogenides.

4. Experimental Section

Attempts at synthesizing phase-pure specimens employing the appropriate binary compounds and procedures previously reported were unsuccessful. For example, a stoichiometric mixture of BaS and SnS reacted at 1073 or 1023 K resulted in the formation of P2₁/c BaSnS₂ as well as $Ba_3Sn_2S_7$, $BaSn_3S_2$, and SnS. An elemental mixture of Ba, Sn, and S combined in the ratio of 1:1:2.2 reacted at 1073 K also proved unsuccessful, resulting in the formation of Ba₃Sn₂S₇ and SnS with no BaSnS₂ present in the final product. Hence, we focused significant effort on investigating a synthetic approach that can produce phase-pure BaSnS2. The synthesis method developed is as follows. High-purity Ba pieces (Alfa Aesar, 99.9%), Sn powder (Alfa Aesar, 99.85%), and ground S flakes (Alfa Aesar, 99.999%) were weighed in a 1:1:2 stoichiometric ratio inside a glove box under a nitrogen atmosphere. The elements were mixed by hand before being loaded onto a quartz crucible and sealed in an evacuated silica ampoule. The elemental mixture was heated up to 1073 K at 15 Kh and held at this temperature for 30 h. The reaction mixture was cooled to 773 K at 2 K h⁻¹, followed by cooling to room temperature at 10 K h⁻¹. Powder XRD data were obtained in Bragg-Brentano geometry using a Bruker D8 Focus Diffractometer, a graphite monochromator, and Cu Kα (1.54056 Å) radiation. Rietveld structural refinement was accomplished using GSAS II^[48] software with preferred orientation included in the refinement. [49–51] SEM on a cracked surface of a representative part of the as-synthesized ingot revealed the grain morphology and size. EDS of the same specimen was performed with an Oxford INCA X-Sight 7582M (INCA software) equipped SEM (JEOL JSM-6390LV). EDS data obtained from several random positions were used to analyze the homogeneity and composition. DTA was performed with a TA Instruments Q600 apparatus. The isobaric heat capacity, Cp, was measured from 1.8 to 250 K using a commercial Quantum Design Physical Property Measurement System (PPMS) with Apiezon N-grease and appropriate addenda. The maximum experimental error within the entire measured temperature range was $\pm 5\%$. UV-vis-NIR diffuse reflectance spectroscopy was performed with a PerkinElmer Lambda 950 equipped with a 150 mm integrating sphere. The bandgap was determined using a Tauc plot of the Kubelka-Munk transform. Photoluminescence was collected using a Renishaw InVia with 514.5 nm Ar⁺ laser excitation and emission detection on a 1" CCD spread of a 1200 lines mm⁻¹ grating. Certain commercial equipment, instrumentation, and materials are identified in this document to adequately specify the experimental procedures. Such identification does not imply recommendation or endorsement by



www.advancedsciencenews.com



the National Institute of Standards and Technology, nor does it imply that the products identified are necessarily the best available for the purpose.

Acknowledgements

This work was supported by the National Science Foundation Grant No. DMR-1748188. We thank O. P. Ojo for Rietveld structure refinements. Specific heat measurements (A.F.M.) were supported by the U.S. Department of Energy, Office of Science, Basic Energy Sciences, Materials Science and Engineering Division. Oak Ridge National Laboratory is managed by UT-Battelle LLC under contract DE-AC05000OR22725. A.J.B. and A.R.H.W. thank Catherine Cooksey (NIST) for use of instrumentation, and Joshua Martin and Dylan Kirsch (NIST) for their assistance with sample preparation.

Conflict of Interest

The authors declare no conflict of interest.

Data Availability Statement

The data that support the findings of this study are available from the corresponding author upon reasonable request.

Keywords

semiconductors, ternary chalcogenides, thermal properties

Received: December 3, 2021 Revised: January 10, 2022 Published online: February 11, 2022

- [1] I. Chung, M. G. Kanatzidis, Chem. Mater. 2016, 26, 849.
- [2] G. S. Nolas, J. Poon, M. G. Kanazidis, MRS Bull. 2006, 31, 199.
- [3] C. Han, Q. Sun, Z. Li, S. X. Dou, Adv. Energy Mater. 2016, 6, 1600498.
- [4] O. Fischer, Solid-State Science, Springer, Heidelberg 1990.
- [5] R. V. Gamernyk, Y. P. Gnatenko, P. M. Bukivskij, P. A. Skubenko, V. Y. Slivka, J. Phys.: Condens. Matter 2006, 18, 5323.
- [6] D. Aldakov, A. Lefrancois, P. Reiss, J. Mater. Chem. C 2013, 1, 3756.
- [7] G. R. Chen, C. H. Li, C. Y. Yu, M. F. Wang, C. S. Lee, *Inorg. Chem.* 2020, 59, 11207.
- [8] F.-J. Fan, L. Wu, S. H. Yu, Energy Environ. Sci. 2014, 7, 190.
- [9] Y. Dong, A. R. Khabibullin, K. Wei, J. R. Salvador, G. S. Nolas, L. M. Woods, Chem. Phys. Chem. 2015, 16, 3264.
- [10] G. S. Nolas, S. M. Hassan, Y. Dong, J. Martin, J. Solid State Chem. 2016, 242, 50.
- [11] Z. Guo, Z. Liu, J. Deng, J. Lin, Z. Zhang, X. Han, F. Sun, W. Yuan, J. Alloys Compd. 2021, 160820.
- [12] W. Shi, A. R. Khabibullin, D. Hobbis, G. S. Nolas, L. M. Woods, J. Appl. Phys. 2019, 125, 155101.
- [13] Y. Dong, H. Wang, G. S. Nolas, Inorg. Chem. 2013, 52, 14364.
- [14] D.-J. Xue, B. Yang, Z.-K. Yuan, G. Wang, X. Liu, Y. Zhou, L. Hu, D. Pan, S. Chen, J. Tang, Adv. Energy Mater. 2015, 5, 1501203.
- [15] H. Lei, J. Chen, Z. Tan, G. Fang, Solar RRL 2019, 3, 1900026.
- [16] M. R. Gao, Y. F. Xu, J. Jiang, S. H. Yu, Chem. Soc. Rev. 2013, 42, 2986.
- [17] Y. Dong, H. Wang, G. S. Nolas, Phys. Status Solidi RRL 2014, 8, 61.
- [18] W. G. Zeier, A. LaLonde, Z. M. Gibbs, C. P. Heinrich, M. Panthöfer, G. J. Snyder, W. Tremel, J. Am. Chem. Soc. 2012, 134, 7147.

- [19] G. S. Nolas, H. Poddig, W. Shi, L. M. Woods, J. Martin, H. Wang, J. Solid State Chem. 2021, 297, 122058.
- [20] K. Wei, A. R. Khabibullin, T. Stedman, L. M. Woods, G. S. Nolas, J. Appl. Phys. 2017, 122, 105109.
- [21] K. Wei, G. S. Nolas, ACS Appl. Mater. Interfaces 2015, 7, 9752.
- [22] R. Woods-Robinson, Y. Han, H. Zhang, T. Ablekim, I. Khan, K. A. Persson, A. Zakutayev, Chem. Rev. 2020, 120, 4007.
- [23] M. Ibáñez, R. Zamani, A. LaLonde, D. Cadavid, W. Li, A. Shavel, J. Arbiol, J. R. Morante, S. Gorsse, G. J. Snyder, A. Cabot, J. Am. Chem. Soc. 2012, 134, 4060.
- [24] C. Zhou, C. Dun, K. Wang, X. Zhang, Z. Shi, G. Liu, C. A. Hewitt, G. Qiao, D. L. Carroll, *Nano Energy* **2016**, *30*, 709.
- [25] R. Gupta, N. Kumar, P. Kaur, C. Bera, Phys. Chem. Chem. Phys. 2020, 22, 18989.
- [26] A. Kojima, K. Teshima, Y. Shirai, T. Miyasaka, J. Am. Chem. Soc. 2009, 131, 6050.
- [27] B. V. Lotsch, Angew. Chem., Int. Ed. 2014, 53, 635.
- [28] N.-G. Park, J. Phys. Chem. Lett. 2013, 4, 2423.
- [29] H. J. Snaith, J. Phys. Chem. Lett. 2013, 4, 3623.
- [30] H. Zhou, Q. Chen, G. Li, S. Luo, T.-b. Song, H.-S. Duan, Z. Hong, J. You, Y. Liu, Y. Yang, Science 2014, 345, 542.
- [31] W. Nie, H. Tsai, R. Asadpour, J.-C. Blancon, A. J. Neukirch, G. Gupta, J. J. Crochet, M. Chhowalla, S. Tretiak, M. A. Alam, H.-L. Wang, A. D. Mohite, Science 2015, 347, 522.
- [32] A. Mei, X. Li, L. Liu, Z. Ku, T. Liu, Y. Rong, M. Xu, M. Hu, J. Chen, Y. Yang, M. Grätzel, H. Han, Science 2014, 345, 295.
- [33] F. Hao, C. C. Stoumpos, D. H. Cao, R. P. H. Chang, M. G. Kanatzidis, Nat. Photonics 2014, 8, 489.
- [34] J. E. Iglesias, H. Steinfink, Acta. Cryst. B 1973, 29, 1480.
- [35] S. Del Bucchia, J. C. Jumas, M. Maurin, Acta Crystallogr., Sect. B: Struct. Crystallogr. Cryst. Chem. 1980, 36, 2935.
- [36] S. Hao, L.-D. Zhao, C.-Q. Chen, V. P. Dravid, M. G. Kanatzidis, C. M. Wolverton, J. Am. Chem. Soc. 2014, 136, 1628.
- [37] Y. Li, L. Wang, Y. Qiao, Y. Gan, D. J. Singh, Phys. Rev. Mater. 2020, 4, 055004.
- [38] M. Hervieu, G. Perez, P. Hagenmuller, Bull. Soc. Chim. Fr. 1967, 6, 2189
- [39] H. Lin, H. Chen, Y. J. Zheng, Y. K. Chen, J. S. Yu, L. M. Wu, Chem. Commun. 2017, 53, 2590.
- [40] Z. Z. Luo, C. S. Lin, W. D. Cheng, H. Zhang, W. L. Zhang, Z. Z. He, Inorg. Chem. 2013, 52, 273.
- [41] C. Kittel, Introduction to Solid State Physics, John Wiley & Sons, New York 1976.
- [42] W. Lai, Y. Wang, D. T. Morelli, X. Lu, Adv. Funct. Mater. 2015, 25, 3648
- [43] M. D. Nielsen, V. Ozolins, J. P. Heremans, Energy Environ. 2013, 6, 570.
- [44] D. Hobbis, H. Wang, J. Martin, G. S. Nolas, Phys. Status Solidi-RRL 2020, 14, 2000166.
- [45] Y. Dong, A. R. Khabibullin, K. Wei, J. R. Salvador, G. S. Nolas, L. M. Woods, ChemPhysChem 2015, 16, 3264.
- [46] A. R. Khabibullin, K. Wei, T. D. Huan, G. S. Nolas, L. M. Woods, ChemPhysChem 2018, 19, 2635.
- [47] P. Makuła, M. Pacia, W. Macyk, J. Phys. Chem. Lett. 2018, 9, 6814.
- [48] B. H. Toby, R. B. Von Dreele, J. Appl. Crystallogr. 2013, 46, 544.
- [49] J. P. Cline, M. D. Vaudin, J. E. Blended, C. A. Handwerker, R. Jiggetts, K. J. Bowman, N. Medendorp, Adv. X-ray Anal. 1993, 37, 473.
- [50] M. M. Seabaugh, M. D. Vaudin, J. P. Cline, G. L. Messing, J. Am. Ceram. Soc. 2000, 83, 2049.
- [51] W. A. Dollase, J. Appl. Crystallog. 1986, 19, 267.